A. Specific Aims

A.1 Introduction. In this proposal, we seek a renewal of previous grant R15HL148842 entitled "Identifying the function of the Fibrin(ogen) alpha-C connector region". The long-term aim of this work is to provide a robust, multidisciplinary training environment for undergraduate students while determining the mechanisms regulating fibrin and fibrinogen function, with the goal of improving the diagnosis and treatment of cardiovascular disease. The previous grant was highly successful, resulting in twelve publications including seven distinct undergraduate authors and three undergraduate first authors. In this proposal, we seek to build on the achievements of the previous proposal and test novel hypotheses that originated from that work.

Fibrin fiber networks (gels) are one of the main components of blood coagulation and wound healing. After the completion of wound healing, blood clots are digested by the enzyme plasmin in the process of fibrinolysis. The polymerization of fibrin has been studied for decades, but the crucial step in this process, the transition from oligomers into a branched fiber structure (commonly referred to as lateral aggregation and branching), is poorly understood. Because this transition is the determining factor in the final clot structure, understanding the mechanisms regulating fibrin polymerization will provide avenues for novel therapeutic approaches that modulate clot structures.

Moreover, while many techniques are commonly used to study fibrin structures, a lack of standardization between techniques creates difficulties in comparing results. Therefore, there is an urgent need for a comprehensive, multi-technique quantization of the structural properties of fibrin gels under varying biochemical conditions that can serve as a baseline for future comparisons. Only with clot structures that have been validated through multiple techniques can a confident correlation be made between polymerization processes and the structures that result from them.

Finally, fibrin structures such as fiber diameter and pore size are known to affect the fibrinolytic process. Since these fibrin structures arise, in large part, from the polymerization process, a strong argument could be made that the polymerization process predetermines a clot's eventual susceptibility to digestion. However, to our knowledge, polymerization processes have not been previously correlated with the fibrinolytic process.

Our fundamental, underlying hypothesis is that early polymerization processes propagate throughout the entire coagulation process, affecting both the final gel structure and fibrin's resistance to enzymatic digestion. To test this hypothesis, we will utilize a novel, interdisciplinary approach, which is rooted in techniques and collaborations developed during the period of our original research proposal. Pursuing these aims will provide invaluable interdisciplinary research experience for students at East Carolina University (ECU), Wake Forest University (WFU), and University of Central Oklahoma (UCO) because it connects concepts in physics, biochemistry, polymer science, mathematics, modeling and medicine. Undergraduate and graduate students at ECU, WFU, and UCO already played an important role in collecting preliminary data for this proposal, and the proposal relies heavily on student involvement to accomplish its aims.

Specific Aim 1: Make direct observations of fibrin polymerization and quantify polymerization processes and kinetics. Using high framerate, high resolution fluorescent microscopy techniques, including Light Sheet Microscopy and widefield microscopy with 3-D computational clearing, combined with advanced image analysis tools, and atomic force microscopy, we will observe and quantify the processes of fibrin polymerization. In particular, we will focus on determining the mechanisms regulating the transition from fibrin oligomers to a fully formed branched gel. In so doing, we will measure rates of fiber growth, changes in fiber stiffness, and branch point formation for the first time. Our experimental results will be tested against a novel, agent-based mathematical model of fibrin polymerization, which is the first model to simultaneously account for thrombin activation of fibrin, polymerization of oligomers, and lateral aggregation and branching of oligomers and fibers.

Specific Aim 2: Validate fibrin structural properties with multiple techniques and correlate the final structural properties of fibrin gels with the early stages of fibrin formation. Using two or more different techniques for each property including turbidimetry, super-resolution fluorescence microscopy, confocal microscopy, and scanning electron microscopy, we will measure fibrin fiber lengths and diameters as well as network pore sizes and branch point densities to cross-validate the structural characteristics of fibrin gels. These network structural properties will be correlated with polymerization processes to identify which aspects of polymerization determine which fibrin structures.

Specific Aim 3: Determine how early clot structures affect lysis. We will measure the fibrinolysis rates of whole networks and individual fibers within the network using novel fluorescence-based microscopy approaches. We will correlate lysis rates with polymerization processes such as fiber growth rates to test our hypothesis that much of the hemostatic process is determined by the early stages of polymerization. By comparing our results with detailed mathematical models of fibrinolysis, we will identify potential mechanisms responsible for the observed correlations.

B. Background and Significance

Progress report/Preliminary study. In this proposal, we are requesting a renewal of previous grant R15HL148842 entitled “Identifying the function of the Fibrin(ogen) alpha-C connector region”. The proposal aimed to provide a robust, multidisciplinary training environment for undergraduate students while studying the underlying mechanisms regulating the structure, mechanical properties, and fibrinolytic susceptibility of blood clots. Herein, we will briefly describe progress towards those aims as well as a rationale for how working towards those aims provided the hypothesis and preliminary data for the proposed study.

We generated recombinant fibrinogen molecules with a truncated αC-connector. We published our methods for expressing fibrinogen transiently and purifying fibrinogen (1). We found that for fibers with the entire connector region deleted (residues 264 – 391 of the α-chain) the extensibility (fracture strain) of uncrosslinked fibers was reduced by a factor of 1.7 (from 2.10 to 1.26), and the modulus (stiffness) decreased by a factor of 3 (from 3 MPa to 1 MPa). Moreover, SEM images showed that variant fibers often formed flat, ribbon-like fibers, failing to form the cylindrical fibers seen in wild type fibers. Data for experimentally obtained stress-strain curves on single fibrin fibers were used by the Barsegov lab to develop a novel, theoretical model of fibrin fiber mechanics. Comparison between model and experimental curves indicated that extension of αC tethers may play a major role in elastic deformations for strains below 160%, while above 160%, unfolding of the coiled coils and γ-nodules becomes important (2). In the current proposal, we intend to continue to use αC variants as part of our study of fibrin polymerization.

Concurrent with our work on the αC region, we also spent significant effort developing methods for fibrin structural characterization. We published three papers towards this effort and currently have another in press. In one paper, Co-I Guthold and collaborators developed standardized methods for interpreting and validating the maximum absorbance (MA) data from turbidimetry analysis of plasma clots (3). In a second paper, we developed and evaluated a measuring tool to determine fiber diameter and porosity measurements of fibrin clots in SEM images (4). In a third paper, we investigated methods for analyzing turbidimetry data for extracting fibrin diameter and compared these theoretical results to experimental data obtained using SEM and super-resolution fluorescence microscopy (5). As part of this structural work, we realized that with light sheet and Leica computational clearing microscopy, we could observe the polymerization of fibrin networks for the first time. This series of results provide the hypotheses and impetus for Aims 1 and 2 in the current proposal, where we intend to investigate mechanisms of fibrin polymerization and develop standardized protocols for determining clot structural properties.

We also made significant advances in measuring fibrinolytic mechanisms. In our first paper (6), we showed that fiber clearance during lysis occurs through multiple pathways including transverse cleavage, bundling, and collapsing. We also showed that inherent fiber tension (tension generated in the fibrin fiber during polymerization) plays an important role during lysis (7, 8). As these results developed, PI Hudson initiated a collaboration with Dr. Brittany Bannish, who has developed detailed mathematical models of microscale fibrinolysis. Dr. Bannish extended her model to include the effects of inherent tension in her results. We developed a novel approach to studying fibrinolysis using fluorescence microscopy, which enabled the first determination of the fibrinolytic cleavage rates of individual fibrin fibers and demonstrated that inherent fiber tension pulls fibers apart (7). Dr. Bannish simulated the diffusion and binding of plasmin molecules during this process, demonstrating how many plasmin molecules are bound to a fiber at a certain time. This fruitful collaboration led to the inclusion of Dr. Bannish as a co-I on this renewal, where she will be continuing to model fibrinolysis (Aim 3 of the current proposal), while also developing models of polymerization (Aim 1).

In summary, our productive work during our initial grant led to novel insights into fibrin polymerization, structure, and fibrinolysis. These results were communicated in twelve publications (list found at end of research proposal), with another in press and more in preparation, and have directly generated the aims of our new research proposal. Most importantly, this investigation provided a fruitful training ground for undergraduate and graduate students. Three published papers had undergraduate first/lead authors, and in total eight different undergraduate students had authorship roles on publications. In addition, students made over a dozen conference presentations. As a highlight, Spencer Lynch was the only undergraduate speaker at the 2021 International Fibrinogen Research Society mini-symposium. While several students who worked on these projects are still enrolled as undergraduates, the ones who graduated have been accepted into or attended respected graduate and medical programs including Duke University (Elizabeth Viverette, Andrew Fuquay, Spencer Lynch), NC State University (Sean Cone), Philadelphia College of Osteopathic Medicine (Justin Litofsky), Wake Forest University (Annie Brigham), University of Florida (Caleb Sawyer), University of North Carolina, Chapel Hill (Ethan Payne). These results demonstrate the positive impact the AREA award had on the research environments of the participating institutions.

B.1 Introduction to new proposal. Fibrin fibers form the structural scaffold of blood clots. Under physiological conditions, fibrin forms at the sites of injury before being digested after the completion of wound healing by plasmin in the process of fibrinolysis. The structural properties of a fibrin network such as pore size and branch point density, and the structural properties of fibrin fibers such as length and diameter, are regulated by many factors including chemical and enzyme concentrations, blood flow rates, and cellular content (such as platelets and tissue-factor bearing cells) (9). Altered fibrin structures have been linked to diseases such as myocardial infarction (10), ischemic stroke (11), venous thromboembolism (12), diabetes (9), and COVID-19 (13). Interestingly, many of these same diseases, including COVID-19 (13, 14), result in hindered or accelerated fibrinolysis. Thus, understanding: 1) the mechanisms by which fibrin structures form, 2) the structural properties of the formed networks, and 3) the connection between polymerization processes and fibrinolysis has the potential to both improve clinical diagnosis and aid in the development of improved treatments.

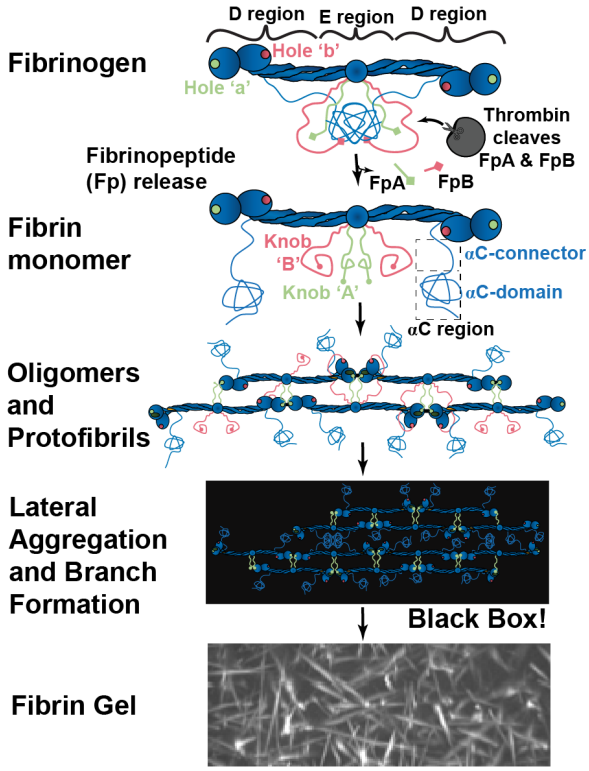

Figure 1. The fibrin polymerization process. Thrombin cleaves FpA from fibrinogen, causing protofibril formation through A:a knob:hole interactions. Cleavage of FpB is thought to promote lateral aggregation and the formation of B:b bonds. The processes of lateral aggregation and branch point formation are poorly understood, but lateral aggregation is thought to occur through the formation of αC polymers between nearby protofibrils. Polymerization results in a 3-D fibrous gel.

The polymerization mechanisms of fibrin have been studied for over 100 years using a multitude of techniques, and the commonly depicted steps of polymerization are summarized in Fig. 1. Despite this longstanding interest, prior limitations in techniques leave large knowledge gaps in understanding the processes and mechanisms governing the transition from small fibrin oligomers to a fully branched fibrin gel.

B.2 Seminal studies of fibrin polymerization and structure. Early light microscopy studies of fibrin polymerization reported bright specks appearing, which grew into rods and consolidated into rigid-looking needles (15). Later, electron microscopy (EM) studies (16, 17) showed that many fibers had a sub-structure, with a lateral banding pattern of ~ 22 nm.

B.3 Fibrinopeptide release and knob:hole interactions. Fibrinogen, a large homodimeric molecule in blood, is converted to fibrin when thrombin cleaves two N-terminal peptides (fibrinopeptide A [FpA] and fibrinopeptide B [FpB]) off its α- and β-chains (18, 19) (Fig. 1). The dimericity of fibrinogen means that each molecule has two FpAs and two FpBs. FpA is removed more rapidly than FpB, but even the two FpAs are released at different rates (20). Release of fibrinopeptides results in the exposure of polymerization knobs 'A' and 'B' which preferentially bind to corresponding holes 'a' and 'b', forming A:a and B:b knob:hole interactions (21).

B.4 The formation of 'protofibrils'. It was proposed that fibrin polymerizes into linear oligomers (often referred to as protofibrils) with partial overlapping fibrin molecules, resulting in two parallel and end-to-end chains with staggered junctions (Fig. 1) (22). The fibrinogen molecule measured ~47.5 nm long, roughly double the length of the fiber banding pattern in early EM images (16, 17). The protofibril model and corresponding structures were extensively studied using electron microscopy (23-25), and histograms of protofibril length showed an increase over time (26). Stop-flow light scattering experiments suggested that protofibrils form through the A:a interactions, protofibril formation occurs prior to FpB cleavage, and FpB removal is a prerequisite for (rapid) formation of fibers and gelation (27). However, protofibrils formed from desA fibrin (only FpA removed) are less ordered than protofibrils formed from desAB fibrin (both FpA and FpB removed) (26), suggesting some role for FpB. EM of fibrin fibers demonstrated that protofibrils in fibers twist around the fiber and account for the fibrin banding patterns (28, 29). More recently, Atomic Force Microscopy (AFM) imaging combined with molecular dynamics simulations have been interpreted to support the protofibril model of assembly (30).

While the protofibril model has the aforementioned support, it does not account for the fact that the two FpAs are released at different rates and other data suggests early fibrin oligomers can have other arrangements. AFM- and EM-based studies demonstrated that fibrin monomers can align end-to-end linearly (31), while electrosprayed EM studies found that the double-stranded protofibrils only comprised ~1-2% of all linear chains (32, 33). X-ray/light scattering studies suggested that initial fibrin forms are thinner than that of a double-stranded

protofibril (34). Two other models of oligomers, the “interlocked single-stranded growth model” (32) and the “y-ladder model” (34) suggest possible non-protofibril fibrin oligomer structures based on the fact that the two FpAs are released at different rates. Thus, while the protofibril model is the widely accepted explanation for the transition from fibrin monomers to oligomers (Fig. 1) there is a need to reexamine these ideas using modern, high-resolution techniques and mathematical modeling (described below).

B.5 The dynamics of fiber formation. The transition from protofibrils (oligomers) to fibers is arguably the least understood part of fibrin polymerization. Light scattering techniques can resolve kinetics but cannot directly visualize fibrin structures, while EM techniques can resolve fine structures but cannot directly measure kinetics.

Turbidity (light scattering at one angle and wavelength) is a technique commonly utilized to study the kinetics of fibrin formation. Early turbidity studies (27) suggested a lag phase (corresponding to protofibril formation), a rapid increase in scattering (corresponding to lateral aggregation of protofibrils into fibers, possibly mediated by the αC region (35)), followed by a plateau phase (corresponding to the fully-formed gel (36, 37)). Studies combining turbidity and electron microscopy suggested that protofibrils must grow to a critical length of ~ 600 nm (~25 monomer/protofibril) in order to nucleate lateral aggregation (38, 39). During and after lateral aggregation, transglutaminase FXIIIa adds covalent crosslinks to fibrin, which help to rigidify the gel (12).

Improvement of light/fluorescence microscopy techniques have enabled limited time-resolved visualization of fibrin polymerization. An early confocal microscopy study visualized 3D fibrin polymers every 2 minutes (40), which enabled the preliminary measurement of fiber thickness and network pore size (the space between fibers) over time. Later, deconvolution microscopy was used in 2D to study fiber maturation after the establishment of a gel (~ 4 minutes after the initiation of polymerization) (41), but fibrin species prior to this point were unable to be analyzed. Later, high frame rate confocal microscopy (stack every 16s) combined with transmission electron microscopy (TEM) was used to study the 2-D diffusion and structure of early fibrin oligomers but fiber branch point formation and growth rates weren’t measured (42). Finally, Total Internal Reflection (TIRF) microscopy was used to study fiber formation “one molecule at a time”, but only radial growth was determined, and the measured fiber diameters were often unusually high (400 - 900 nm) (43). To our knowledge, these four studies comprise the entirety of microscopy-based studies of fibrin polymerization, however fiber lengthening and branching remain unresolved and an understanding of how different biochemical conditions (e.g., fibrinogen and thrombin concentrations) alter these processes remains unexplored through microscopy. Our preliminary data (Figs. 2-7) demonstrate our ability to clarify these processes.

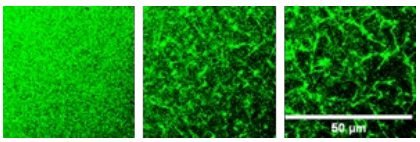

Figure 2. Clot polymerization. Time series captured using a Leica THUNDER microscope. T = 0, 36, 60 s. Scale bar, 50 μm.

B.6 Branch point formation. The origin and structure of fiber branch points (the locations where fibers come together in the network; alternatively referred to as junctions) has received much attention but remains elusive. The structure of branch points has been debated, with some studies claiming 4-6 fibers coalesce at “nodes” (16, 44, 45), while others show three-fiber branches with either one fiber splitting into two strands (bilateral junctions) (46, 47) or with branch points forming from three fiber segments of roughly the same size with the protofibrils twisted around each other (equilateral junctions) (47, 48). A recent study suggested that fibrin branch points are highly dependent on fibrin “aggregates” (49) and mechanical studies of branch points show that they break at the same frequency as fibers and do not “unzip” (50). Hypothesized origins of branch points include adjacent interprotofibril separation (bilateral) (47) or intraprotofibril branching due to an incorrectly bound fibrin molecule (equilateral) (34, 51, 52). Our preliminary data (D.1.5) novelly suggests that fibers can also form branches by growing into each other, perhaps explaining the origins of “nodes”. Our preliminary data notwithstanding, observations of branches forming are nearly non-existent, thus the mechanisms of their formation remain a mystery. Because the branching process plays such a dramatic role in determining the later clot architectures, it is vital for a comprehensive scientific model of this process to be developed.

B.7 Models of fibrin polymerization. Computational models have been employed to help understand the mechanisms and kinetics of fibrin polymerization and branching (53). The models can broadly be classified as differential equations (DE)-based (37, 52, 54-58), molecular dynamics (MD)-based (59, 60), or mechanics-based (61, 62). The DE models are used to understand polymerization and branching at a macroscale, and do not account for fine-scale structural details of fibrin monomers. Conversely, MD models carefully account for shape, structure, and extensibility of fibrin monomers, but are computationally intractable at larger spatial or temporal scales. A mesoscopic model of protofibrils undergoing Brownian motion (61) essentially “splits the difference” between MD and DE models, but by starting with preformed protofibrils, excludes important information about thrombin-induced activation of fibrin and polymerization of protofibrils. Similarly, a constitutive model of a maturing fibrin network describes viscoelastic properties of the network, but assumes a preformed clot and thus ignores the important fibrin activation and polymerization steps (62).Thus, to test different hypotheses of

polymerization and branch point formation and to better understand how these conditions affect clot structure and lysis, there is a need for a comprehensive mathematical model of fibrin polymerization and branching.

B.8 Fibrinolysis and fibrin structure. Previous studies have investigated the link between fibrin structure and fibrinolysis rates. Typically, clots composed of thinner, more closely spaced fibers are more resistant to fibrinolysis (63, 64); however, thin fibers are more rapidly cleaved than thick fibers (65, 66). We previously used mathematical modeling to propose that the relationship between clot structure and lysis rate depends on the ratio of fibrinolytic molecules per unit area at the lysis front (67) and developed the first assay for observing the lysis of individual fibers (7). Because fibrin structures are directly related to polymerization processes, we hypothesize that polymerization in some ways “predetermines” fibrinolytic outcomes, but we are unaware of studies that directly link polymerization processes to lysis rates.

B.9 Conclusions and hypotheses. As detailed in the preceding paragraphs, there remain large knowledge gaps regarding the structure of early oligomers, the processes by which oligomers form fibers (lateral aggregation), and the branching of fibers into networks. We propose to use a suite of modern techniques and modeling methods to study these processes, which will provide a much more nuanced and complete picture of fibrin polymerization. Features that define the fibrin network include fiber length and diameter, branch point density, and pore size. Using multiple modern techniques, we will cross-validate these structural properties of gels to provide a set of standardized network properties under differing biochemical conditions. Finally, our overall hypothesis is that early stages of fibrin polymerization propagate forward and predetermine fibrin clot structure and clot lysis rates. By connecting lysis mechanisms to structural properties and polymerization mechanisms, we can obtain a complete understanding of how thrombotic diseases which affect polymerization propagate through the entire hemostatic process.

Our research team provides strong expertise to tackle these questions. Lead PI Nathan Hudson has studied fibrin structures and fibrinolysis for 15 years and serves on the board of councilors for the International Fibrinogen Research Society (IFRS). He has collaborated for the past 5 years with Co-I Dr. Guthold, who has developed numerous Scanning EM (SEM) (4) and AFM-based methods (2, 68-71) for studying fibrin structure and mechanical properties, and is the current president of the IFRS. Their collaborative work formed the basis of the original R15 grant, which resulted in 12 publications and >20 conference presentations. Co-I Dr. Bannish is one of the leading modelers of fibrinolysis and has collaborated with Dr. Hudson over the past 5 years to develop novel models and techniques to understand fibrinolytic mechanisms. Our preliminary data show strong evidence that we can utilize innovative, modern techniques such as light sheet and super-resolution microscopy and enhanced AFM, combined with mathematical models to tackle these questions. The investigators are each passionate about undergraduate research mentorship, come from an R15-eligible institution, and combined have mentored over 40 undergraduate students in the past 5 years. The techniques utilized in this proposal are accessible to undergraduate students and some of the preliminary data was acquired by undergraduates.

C. Innovation

Despite clear correlations between fibrin structures and pathology, there are still large gaps in our understanding of how fibrin structures form and how the polymerization process propagates into network structures and fibrinolysis. In this proposal we will utilize an innovative combination of modern microscopy techniques and mathematical models to gain novel insights into these processes.

C.1 First direct measurements of 3-D fiber growth kinetics. As our preliminary data (D.1.4) demonstrate, using light sheet microscopy and widefield microscopy with computational clearing, we can measure both the radial and longitudinal growth rates of fibrin fibers in three dimensions due to the unprecedented time resolution (3-6s per z-stack). These measurements have distinct advantages over previous 2D measurements of growth kinetics, providing significantly less out-of-focus fluorescence and the ability to rapidly collect large z-stacks. In addition, we are developing novel techniques to measure fiber lengths, which account for changes in fiber flexibility over time. These approaches are being pioneered by UG students in the Hudson and Guthold Labs.

C.2 First measurements of the development of fiber tension. Fibrin fibers have inherent tension that develops during the polymerization process and plays important roles in the fibrinolytic process (6, 7, 29). The origins of this tension are unknown. Based on our preliminary results (D.1.3), we observe fibers developing tension over time, transitioning from a loose, floppy state to a stiff, straight one, and we propose a novel method for determining the stiffness of fibrin fibers using their change in persistence length. By observing these processes under different biochemical conditions, we will determine the mechanisms undergirding the development of fiber tension.

C.3 Direct quantification of fibrin branch point formation. The process of fibrin branching is almost entirely unexplored experimentally. Our preliminary data (D.1.5) suggest that, contrary to most models, fibrin fibers grow without branching, and that branches form when fibers grow/diffuse into each other. We will test whether this

process holds under other biochemical conditions, as it is well known that fibrin branching structures can be dramatically different based on the fibrinogen/thrombin ratios.

C.4 Direct measurements of the role of FpA and FpB removal in polymerization and fibrin branching. While evidence suggests that FpA removal facilitates protofibril formation and FpB removal promotes the formation of a fibrin gel, measurements of these effects are often indirect. In this research, we will directly observe fibrin gel formation in the absence of either FpA or FpB removal, allowing a direct quantification of the rates of fiber growth and branching in the absence of these events.

C.5 Standardization of methods used to characterize fibrin structural properties. While fibrin structural properties have been studied for decades, it is often difficult to compare results between studies due to a lack of standardizations between techniques. Here, we will measure fibrin structural properties including fiber length, diameter, network pore size, and branch point density using at least two techniques, which will provide a much-needed standardization across techniques. We will then correlate the final structural properties to polymerization rates to determine how polymerization processes determine final structures.

C.6 Development of the first comprehensive mathematical model of fibrin polymerization, aggregation, and branching. Existing models of fibrin polymerization either do not include all the detailed steps of the process or are too computationally heavy to run for physiological length and time scales. We will develop the first agent-based model of fibrin polymerization, which will simultaneously incorporate thrombin-induced activation of fibrin, fibrin polymerization into oligomers, and lateral aggregation and branching of oligomers and fibers. This will be the first model to distinguish different branching pathways (bilateral, equilateral, and nodes), as well as the first to attempt to bridge the gaps between early stages of polymerization, resulting clot structure, and subsequent clot lysis.

D. Approach

D.1 Aim 1: Directly observe fibrin polymerization and quantify polymerization processes and kinetics

D.1.1 Introduction and hypothesis. As discussed in the background, fibrin polymerization has been studied for over a century, yet key knowledge gaps remain. The generally recapitulated model is shown in Fig. 1. However, the processes between protofibril formation and the gelation of a 3-D network remain poorly understood. Moreover, alternative theories to oligomer formation including the Y-ladder model (34), the interlocked single-stranded model (32), and the end-to-end model (31) make predictions about the formation of fibrin branching that can be tested and modeled using new approaches. As described below, our preliminary data reveal intermediate steps in the formation of network gelation.

We hypothesize that fibrin fibers start as soft, semiflexible strands rapidly diffusing in solution before growing both longitudinally and radially until colliding with other fibers, after which the fibers continue to grow radially, but not lengthwise. Branch points primarily form from collisions and adhesion between other fibers rather than from the splitting off of single fibers as has been previously suggested. Moreover, we hypothesize that the local (bio)chemical environment determines the extent to which oligomer formation and fiber longitudinal growth, radial growth, and branching are active at particular timepoints during polymerization. To test the effects of biochemical environment on these processes, we intend to study polymerization using 0.5, 1, 3 mg/mL fibrinogen (concentrations covering a range of pathological and physiological conditions (72, 73)) and either 0.1 or 1 U/mL thrombin (unless described otherwise).

D.1.2 Image and model early stages of fibrin polymerization. An AFM can achieve nanometer resolution on soft, biological samples, such as DNA and proteins, without fixation, dehydration, desiccation or coating, in buffer or ambient conditions. We will use AFM to image snapshots of the early stages in fibrin fiber assembly from monomers to dimers to oligomers, including branching, and up to early fiber network formation. A variety of conditions will be used to investigate how conditions affect the prevalence and evolution of any given structure. Previous work (31, 74-76) demonstrated the feasibility of AFM imaging of fibrin(ogen) monomers, fibrin oligomers, protofibrils, and fibrin fibers. However, much of this work focused on resolving subdomains of fibrin(ogen), e.g., the αC region, and not on characterizing and quantifying the different stages and evolution of oligomer and fiber formation, as proposed here.

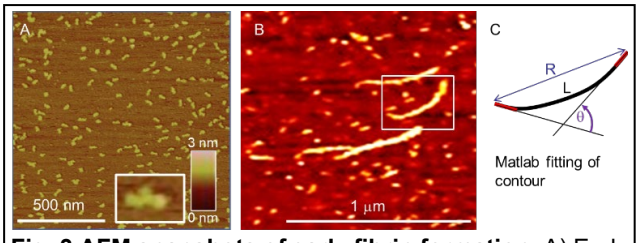

Fig. 3 AFM snapshots of early fibrin formation. A) Early time point showing mostly fibrin(ogen) monomers (see inset). B) Later time point showing the formation of protofibrils. C) Oligomer contours will be fit in Matlab with a polynomial, allowing analysis of the persistence length.

To catch the polymerization process at different stages, we will start the reaction at near physiological conditions (1 mg/ml fibrinogen, 0.1 U/ml thrombin), then dilute the reaction 500x to stop it, and deposit the sample immediately on the substrate. Time points will be taken at 0.5, 1, 2, 5, 10, 20 minutes. Fig. 3A shows a reaction stopped at 1 min. Clearly

visible are individual fibrin molecules with a length of 45 nm, and some dimers. The image was taken by undergraduate student Jesse Gao (Guthold lab). The different assembly paths will be controlled by varying conditions (thrombin:fibrinogen ratio, thrombin substitutes (e.g., batroxobin), fibrinogen variants, and buffer conditions), as outlined below (D1.3, D1.6, D1.7).

D.1.3 Determine the fiber stiffness (persistence length) as a function of time.

Fibers have long been classified as semi-flexible biopolymers, but in many confocal images of fully formed clots they appear straight. Often, after fiber cleavage during lysis, fibers return to a loose, flexible state (7, 77). We hypothesize that the straightness of fibers in polymerized clots has two origins: 1) the flexural rigidity of the fibers (how resistant the fibers are to bending) and 2) inherent tension in the fibers due to polymerization (6, 7, 78). For the first time, we will directly quantify the transition from "flexible" to straight fibers using both atomic force and fluorescence microscopy. The persistence length, P, is defined as the decay length over which a polymer appears straight (Fig. 3C), such that the mean cosine of the angle of deviation, θ, between to segments

$$\langle \cos\theta\,(\ell)\rangle = e^{-\frac{\ell}{2P}}, \qquad (1)$$

where ℓ is the separation between segments. For a larger persistence length, the angle of deviation is smaller. Using polymer statistics, as outlined in our publications (70, 71), the persistence length also relates the mean squared end-to-end distance, $\langle R^2 \rangle$, to the contour length, L, of the polymer (Fig. 3C)

$$\langle R^2\rangle_{2D} = 4PL\left[1-\frac{2P}{L}\left(1-e^{-\frac{L}{2P}}\right)\right]. \quad (2)$$

We will determine oligomer persistence length from AFM images by using techniques that we previously developed for studying DNA persistence length (70, 71). L, R, and θ will be measured by tracing the contours of molecules and applying a polynomial fitting routine in the Matlab program "Alex" (70). Fitting $\langle R^2\rangle$, L, and $\langle \cos\theta\rangle$ values to these equations yields highly accurate values for the persistence length as shown by us (70, 71). Eq. (1) & (2) are valid for equilibrated molecules on a 2D surface; they are also valid for 3D molecules, except that 2P needs to be replaced with P (71).

Significantly, the persistence length can be used to calculate the Young's modulus, Y, of the investigated polymer (70, 71),

$$YI = k_B TP, \quad (3)$$

(I is the 2nd moment of inertia, k_B Boltzmann constant, T temperature), allowing a comparison of the thusly calculated modulus with our macroscopic measurements of fibrin fiber modulus (69). We will use equations (1), (2) and (3) to determine, for the first time, the persistence length, P, and the Young's modulus of protofibrils from AFM images. Preliminary data yield P ~200 nm and a modulus Y ~ 20 MPa, assuming a 2nd moment of inertia I ~ 80 nm^4.

Using similar reasoning, but in 3D, fiber persistence length will be quantified over time from fluorescence images (Fig. 4A-D). To achieve this, we will use modern microscopy techniques that achieve high frame rates including the MuVi SPIM light sheet microscope (Bruker) and Leica THUNDER computational clearing microscope (Leica THUNDER Live Cell Imaging System). ECU researchers have collected a large initial dataset on a MuVi SPIM (79) system, which was used for the preliminary data in this grant, while WFU utilized their recently acquired Leica THUNDER system (80). These instruments have superior 10-100x faster time resolution than laser scanning confocal microscopy, with similar spatial resolution, however the MuVi SPIM system has better depth resolution and less background fluorescence than the THUNDER system. In testing at Wake Forest, the Leica THUNDER captured a 212 μm x 212 μm x 5 μm volume in 3 s while a comparable volume on a Zeiss 880 laser scanning confocal would take over 100 s.

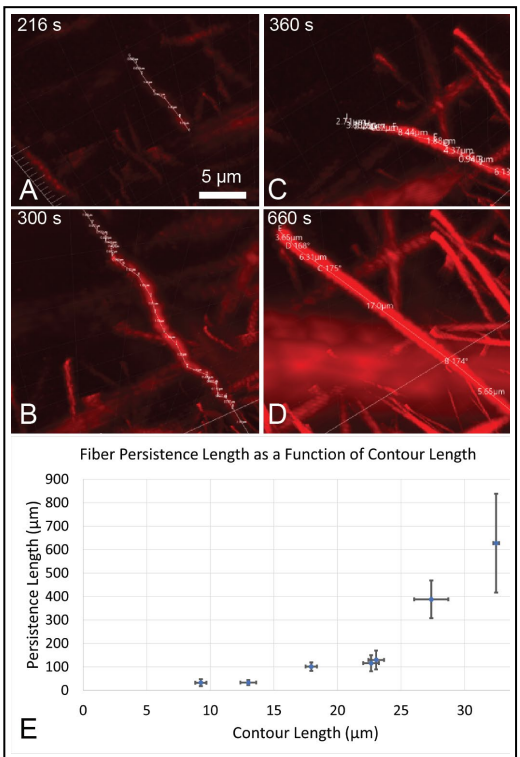

Figure 4. Increasing stiffness/tension of a fibrin fiber. A single fibrin fiber is tracked over time using light sheet microscopy. The fiber transitions from being loose and bendable at early time points (A&B) to stiff and straight at later time points (C&D). Polymerization was initiated with 0.5 mg/mL fibrinogen and 0.1 U/mL thrombin. Fiber persistence length as a function of contour length was estimated for 6 fibers over time, demonstrating that as fibers mature (become longer), they become stiffer.

Polymerization will be initiated by mixing fibrinogen (spiked with 1-2% Alexa Flour™ 488-labled fibrinogen) with thrombin and fibers will be imaged over time. As seen in Fig. 4, early time fibrin fibers show strong deviations from linearity (without significant blurring), while later time fibers appear straight. Because the frame rate of the microscope is fast enough to capture thermal fluctuations of the fibers, the persistence length can be determined from the images using the same methods as described above from the AFM images, except that the analysis is

done in 3D and the 2P in equations (1)-(2) is replaced with P (71). Preliminary data in Fig. 4E demonstrate that the persistence length can be calculated from microscopy images and that the persistence length increases over time as the fibers mature and grow longer. Importantly, the persistence length value of the mature fiber ~ 1mm, corresponds to a Young's modulus of 1 MPa (with diameter ~100 nm), which is in agreement with fiber moduli we have previously calculated by pulling a fiber with the AFM tip (69, 81), providing validation of this approach.

To ensure statistical rigor, we will perform measurements on 100 or more oligomers at each time point described in D.1.2 and will measure fiber stiffness over time for at least 30 fibers for each of the biological conditions described in D.1.1. Taken together, the AFM and fluoresce experiments will enable us to measure the persistence length and Young's modulus for fibrin oligomers, nascent fibers and mature fibers, and thereby determine the progression of stiffness through these different stages. A comparison of the stiffness of fibrin structures will enable us to draw conclusions about the assembly process. For example, if oligomers are stiffer (larger modulus) than mature fibers, as the preliminary data above indicate (20 MPa oligomer vs. 1 MPa fiber), this would imply 'soft' connections between oligomers to form mature fibers.

D.1.4 Measure and model the radial and longitudinal growth rate of fibrin fibers. Microscopy-based dynamics studies indicate that early fibrin forms have a high rate of diffusion, and then elongate into rod-like structures before branches form (41, 43). However, these studies lacked the combined temporal and spatial resolution required to capture fiber growth prior to network formation and the actual process of branch formation, thus the critical transition from oligomers to a fully gelled structure remains underresolved. Moreover, mathematical models of this process tend to focus on broad gelation kinetics (52, 56, 57, 82) or detailed interactions between individual monomers (59, 60), and thus do not explicitly report the dynamics of fiber length and diameter. One early model looked at some of these kinetics (37), but as an ODE model, was unable to investigate spatial heterogeneity or the effect of diffusion.

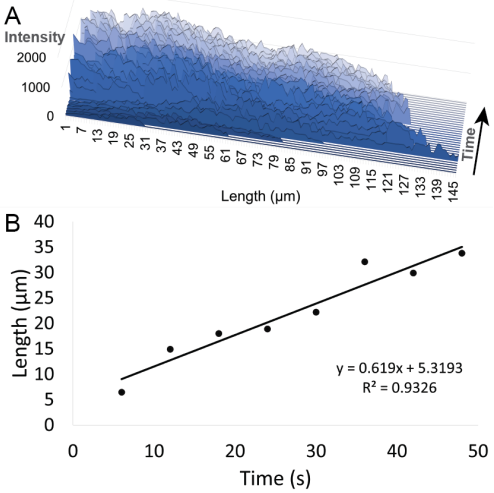

Figure 5. Quantifying the growth rates of fibers. A) 3D plot of Muvi SPIM light sheet microscopy data of fibrin polymerization with y-axis showing the longitudinal intensity, x-axis showing the fiber length, and z- axis showing time (into the page is forwards in time). B) Plot of fiber length over time. Slope of the plot is the growth rate of the fiber. Time starts at the earliest point that the fiber can be detected and continually tracked.

D.1.4.a Directly measure fibrin fiber growth rates. Using MuVi SPIM and/or Leica THUNDER microscopy, we will directly quantify the rates of fiber growth during polymerization starting from the diffusion of fibrin strands to the formation of a branched 3D structure. We will collect polymerization data using the biochemical conditions described in D.1.1. Using Imaris (Bitplane, AG/Oxford Instruments) or similar software, the fluorescence intensity along the length of a fiber will be measured at each timepoint (every 3-6 s). Plots of intensity vs time, such as Fig. 5 will be generated for 30 fibers. From these plots the longitudinal and radial growth rates will be calculated.

By measuring the growth rates of at least 30 fibers for each fibrinogen condition (D.1.1), we will compare growth rates as a function of concentration. Preliminary data (Fig. 5B) show that fibers grow longitudinally at rates ~0.6 μm/s. Simultaneous with the longitudinal growth, the fiber begins to grow radially as evidenced by the increasing intensity (Fig. 5A). Eventually the length plateaus, which is followed by further radial growth. Intriguingly, we observe fiber fragments of high fluorescence intensity joining and forming longer fibers (Fig. 7, purple arrow), suggesting that this mechanism also contributes to fiber growth. We will quantify the fraction of fibers that form through the combining of fiber fragments as opposed to the continual outward growth of a single fibrin fiber. Because fibrin growth kinetics are commonly studied using turbidity (see B.5), we will also study clot formation using this technique under identical biochemical conditions to compare with our microscopy. This initial analysis was done, in part, by undergraduate student Brandon Damgaard at ECU.

D.1.4.b Model fibrin growth rates and correlate with experimental rates. To understand the mechanisms governing experimental results, we will create a novel 2D agent-based model (ABM) of fibrin polymerization. ABMs are a natural way to represent biological processes that occur over multiple time and spatial scales. In an ABM, autonomous individuals (agents) stochastically update their status every time step based on a set of rules. Our model (Fig. 6) will start with a collection of 45-nm long rods (representing fibrinogen monomers) and 5-nm diameter discs (representing thrombin molecules) randomly distributed and oriented in the 2D spatial domain. The rods will include holes 'a' and 'b' and knobs 'A' and 'B' (which will be exposed by thrombin cleavage of fibrinopeptides A and B to create fibrin), and which can interact with knobs and holes on other monomers. The five different types of agents (fibrinogen, fibrin, oligomers, fibers, and thrombin) will be governed by different

rules. All types of agents will diffuse throughout the domain with the appropriate diffusion coefficient. When the necessary agents are within a given distance and/or angle, with some probability that depends on reaction rates: a thrombin molecule can cleave FpA or FpB on a fibrinogen monomer to create fibrin; two fibrin monomers can polymerize to create a new dimer (and repetition of this process can create oligomers of any length); monomers and oligomers can laterally aggregate to create thicker fibers; monomers, oligomers, and fibers can interact in multiple ways to form branches.

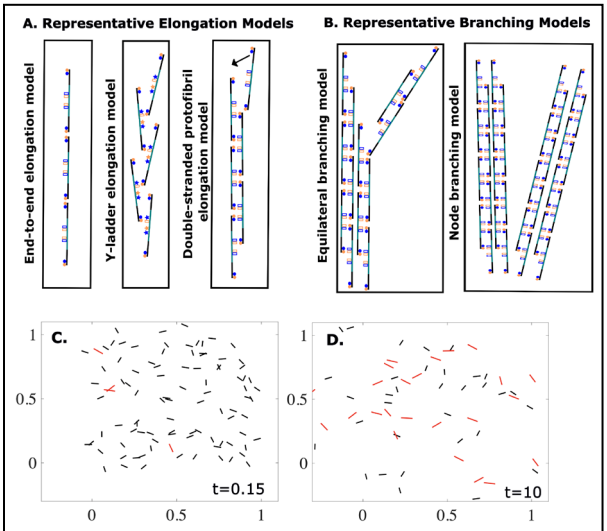

Figure 6. Agent-based model schematic and preliminary results. Representative fibrin oligomer elongation (A) and branching (B) models that will be tested with the ABM. Preliminary ABM results at (C) early and (D) later nondimensional time points. Fibrin monomers (black) can polymerize to form a fibrin dimer (red) if the 2 monomers are within a threshold distance and angular orientation. Dimers are 1.5-times longer than monomers, due to the half-staggered manner in which fibrin polymerizes. As time progresses, more of the monomers have polymerized, and the fibrin has diffused throughout more of the domain.

The "given distances", "probabilities", and "given angles" described above are parameters in the model. As far as is possible, they will be chosen based on known biology and kinetics, but they can also be tuned to determine how the system reacts to different inputs. Information about each individual agent will be updated and stored throughout the simulation, e.g., the width of each fiber, how many and which fibrinopeptides have been cleaved from each fibrin monomer, etc. The model will be simulated using custom built Matlab code and/or ABM software such as NetLogo, BSim, or FLAME.

We built a proof-of-concept model in Matlab in which linear fibrin monomers with random orientation diffuse, rotate, and – when within a given distance and angular threshold – polymerize with other monomers. Results of this preliminary model (Fig. 6) show that we are well equipped to build the full model proposed above. The model will be used to complement, inform, and help explain experiments. Specifically, we will use the model to understand how long oligomers grow before they laterally aggregate. We will compare the model and experimental radial and longitudinal growth data. Importantly, we will also use the model to test different polymerization (linear vs. Y-ladder) and branching (bilateral, equilateral, and nodes) pathways (Fig. 6), to determine which are most likely driving observed experimental polymerization. We will change model parameters and/or rules to determine which conditions give the closest match to experimental data. We hypothesize that the model conditions best fitting the experimental data correspond to the actual physiological conditions.

D.1.5 Formation of fibrin branch points. Fiber branching has not been captured in real time, and there are several competing models as to why fibers branch (34, 47, 52) and for the structure of the junctions between fibers (see B.6 and Fig. 6). Using light-sheet and Leica THUNDER deconvolution imaging, we will image and quantify the process of branch point formation for the first time and correlate this with high resolution AFM images of branch structures. Based on our preliminary data (Fig. 7), we hypothesize that there are at least two mechanisms for the formation of fiber branches: 1) the growing of two or more fibers independently, which then collide, stick together, and form a branch; and 2) the splitting of one fiber into two fibers.

Using techniques described in D.1.2, AFM will be utilized to obtain high resolution images of fiber branch points in early oligomers to determine the structural arrangement of protofibrils. Branches will be categorized as equilateral, bilateral, or node (47) and the relative ratio of each species will be quantified. We will correlate the types of branches in AFM images with the mechanisms of branching observed in fluorescence-based experiments for each biochemical condition described in D.1.1.

Fluorescence based branching experiments will be performed using the same approach as described in D.1.3. From fluorescent image sequences we will identify at least 100 branching events (Fig. 7) for each experimental condition described in D.1.1. Using ImageJ or Imaris, images of branching events will be analyzed, and these events will be separated via the mechanism used to create the branch and the type of branched structure. Branching parameters such as the angles between the fibers and fluorescence intensity at the branch (corresponding to fibrin density) will be quantified.

Finally, recent results suggest that the presence/absence of fibrin aggregates dramatically alters the structure of fibrin branches (49). We will perform experiments at 1.0 mg/mL fibrinogen, 0.1 U/mL thrombin but with and without fibrin aggregates present (many fibrin preparations contain a small amount of aggregates that can be removed with gel filtration). We will perform the same analysis with fluorescence microscopy and AFM and determine the mechanisms by which aggregates regulate the branching process.

The model described in D.1.4.b will be used to help understand how long protofibrils get before they form a branch point and to delineate the contributions of different oligomer structures. We will adjust rules and probabilities in the model to account for the competing elongation and branching theories and collect simulated data about the lengths of oligomers and fibers at the time of first branching. By comparing these data to experimental data, we can propose the most likely branching mechanism, as well as comment on the average length a protofibril reaches before branching occurs.

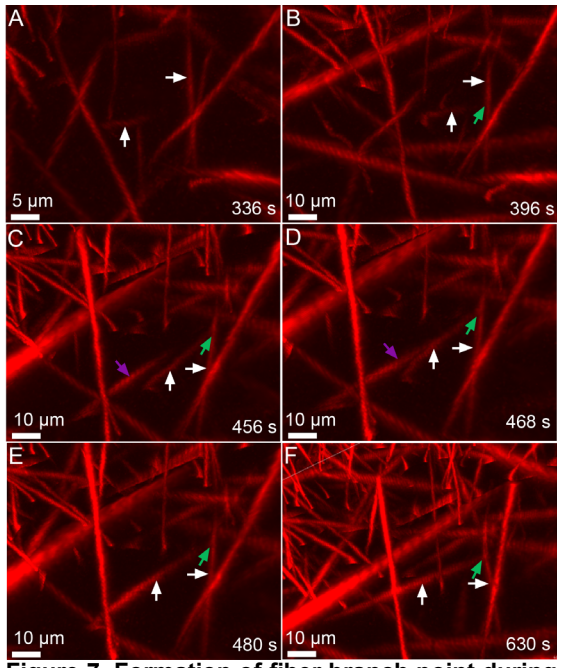

Figure 7. Formation of fiber branch point during polymerization. Panels A-F show a time series, with data taken using a light sheet microscope, of a junction forming when two fibers (white arrows in each image) diffuse together and bind to form a junction (green arrow). The junction first forms in panel B. In panels D-E, a second fiber (purple arrow) binds to another fiber, already in the junction, making it longer and thicker.

D.1.6 Investigate effect of A:a and B:b interactions of fibrin polymerization. In addition to the varying thrombin and fibrinogen concentrations, we will also polymerize and analyze clot formation using the methods described in D.1.2-D.1.5, but we will modify/inhibit specific polymerization reactions. We hypothesize that through inhibiting these interactions, we will observe different early oligomer stages (D.1.2), clot polymerization rates (D.1.4), branch points (D.1.5), structures (D.2), and lysis outcomes (D.3). Key interactions and agents to modify polymerization will be: 1) Use knob 'A' and/or knob 'B' mimicking peptides (GPRP/GHRP) at varying concentrations to occupy hole 'a' and/or 'b' during polymerization so that FpA and FpB are released after thrombin cleavage, but the knob:hole interaction is inhibited. 2) Instead of thrombin, use Contortrixobin (MyBiosource.com), which only releases FpB (83). Thus, the A:a interaction is not activated, but FpB release, which participates in lateral aggregation, will occur (73). 3) Instead of thrombin, use Batroxobin (Pentapharm), which only releases FpA (84). The B:b interaction is, thus, not activated and FpB release will not occur. The agent-based mathematical model parameters and rules will be adjusted to account for the different types of fibrin monomers (e.g., only lacking FpA) and simulation results will complement and inform the experiments.

D.1.7 Investigate the role of the fibrin αC region in polymerization. As part of the original grant, we developed fibrinogen molecules with truncated αC regions. Specifically, we developed fibrinogen variants with partially or fully-deleted αC-connector regions (α chain residues 221-391). Using these variants, we will perform the same experiments as described in D.1.3-D.1.5. The αC region is hypothesized to participate in the lateral aggregation of protofibrils (35), and as such, we anticipate measuring slower polymerization kinetics with these variants. We hypothesize that the fiber stiffness (D.1.4) and branch point formation (D.1.5) will also be affected.

D.1.8 Alternative approaches. Our preliminary data strongly evidence the potential of the described experimental approaches. Much of the preliminary data has been analyzed by hand, but the throughput could be enhanced using automated fiber tracking algorithms in ImageJ (85) or Imaris. We directly have access to the Lecia THUNDER system at Wake Forest, while we intend to use an external resource (Notre Dame imaging core) to collect additional light sheet data, although we have a large (2 TB) initial light sheet dataset that has been utilized for the preliminary data. Time permitting, we could also compare the polymerization processes of fibrin in plasma vs purified fibrin and with and without FXIIIa, as data suggest that fibrin gel structures are different under these conditions (86, 87). Additionally, fibrin assembly depends on the diffusion of the reactants. We could experimentally alter diffusion during polymerization by using different additives such as glycerol (0-50%) or dextran to vary the solution viscosity by up to a factor 5. We predict this would alter the processes of fibrin oligomer formation and lateral aggregation. Changing model diffusion coefficients is as straightforward as adjusting the distance a given agent is allowed to move in a fixed timestep.

In the event that the proposed ABM does not perform as expected, or is computationally intractable for the timescale of interest, we will pursue two different options: 1) modify the Weisel and Nagaswami ordinary DE model (37) to a partial DE model that accounts for diffusion, and 2) create a stochastic reaction-diffusion model. The creation of a PDE model is straightforward and would be fast to implement. Since all individuals within a given class (e.g., fibrin molecule or fiber) are assumed to be homogeneous in a DE model, we will lose some information about variability, but the model will be significantly less computationally intensive than the ABM. The stochastic model would be implemented using the Gillespie algorithm (88), but because only one reaction can happen each timestep, many tiny timesteps would be necessary and thus this model could take just as long (or

longer) to run than the ABM. Implementing the tau-leaping Gillespie variant may speed up the computation. Additionally, the ABM model assumes that fibrinogen is a rigid rod, but fibrin is known to be flexible (89). We can modify the model to allow the molecule to have a hinge in the middle. This will create another degree of freedom, and potentially result in fibrin networks with different properties. By comparing results from this "hinged fibrinogen" model to those from the original model, we will identify the network properties that are most sensitive to the flexibility of fibrin.

D.2 Aim 2: Validate fibrin structural properties with multiple techniques and correlate the final structural properties of fibrin gels with the early stages of fibrin formation

D.2.1 Introduction and hypothesis. Although fibrin gel structures have been studied for decades using a variety of techniques, comparing results between studies and techniques is often challenging because many techniques require unique sample preparations or concentrations. Because of this, there is a key knowledge gap in understanding the conditions under which different techniques will provide congruent results. In addition, the proliferation of super-resolution microscopy over the past decade provides a novel approach for studying fibrin structures, but there has not been a careful comparison between structures observed with super-resolution microscopy and those seen with previously common techniques such as scanning electron microscopy. We hypothesize that the gel structures at the end of polymerization directly result from the early and intermediate fibrin structures described in Aim 1.

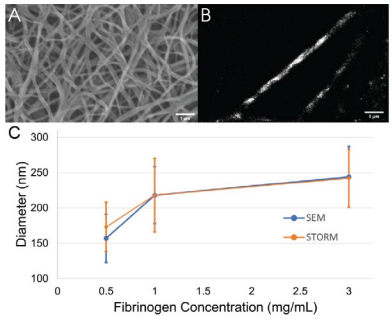

Figure 8. Comparison of fibrin fiber diameters. Representative images of fiber diameters obtained using two different techniques, A) scanning electron microscopy, and B) super-resolution STORM fluorescence microscopy. C) Comparison of fiber diameters for a thrombin concentration of 0.1 U/mL.

We will perform the first comprehensive, multi-technique validation of fibrin structural properties across the range of physiologically relevant biochemical conditions described in D.1.1 (90). Each property (e.g., fiber diameter) will be measured using at least two techniques to corroborate results. By correlating the final gel structures with the early properties of gels (e.g., early fibrin structures from D.1.2 and fiber growth rates from D.1.4), we will make direct determinations of the relationships between the processes operating at these different timepoints and the resulting final structure.

D.2.2 Test the congruence between fibrin fiber diameter measurements using super-resolution microscopy, turbidimetry, and SEM. Altered fibrin fiber structure is linked to pathological states including coronary heart disease, ischemic stroke, and atherosclerosis. In this aim we will test the congruence in measured diameter using three different approaches: STORM (Stochastic Optical Reconstruction Microscopy) super-resolution microscopy, Scanning Electron Microscopy (SEM), and turbidimetry. Polymerization with 2% Alexa fluor™ 488-labeled fibrin will be performed as described in D.1.4 for the various biochemical conditions. For SEM, samples need to be fixed and dried, while STORM and turbidimetry are performed on samples in aqueous environments, thus providing a good test for how sample preparation/handling affect the measured fibrin diameters. Multiple techniques have been developed for analyzing turbidimetry data and we previously did a theoretical comparison of the validity of each technique (5). As part of this aim, we will test each of these turbidimetric analysis techniques against each other and against the STORM/SEM data to determine which provide the most similar results. Finally, we will correlate fiber diameters with the early fibrin species and growth kinetics observed in Aim 1 to determine how these early polymerization processes culminate in the final observed diameters.

Preliminary data (Fig. 8) demonstrate a proof-of-concept comparison between fiber diameters obtained from SEM and STORM imaging for several fibrinogen concentrations. The data indicate a strong congruence between the results under these conditions. Data will be collected and analyzed for over 100 fibers and at least three biological replicates at each concentration to ensure statistical rigor.

D.2.3 Fiber lengths, pore size, and branch point density using light sheet and confocal microscopy. While both light sheet microscopy and confocal microscopy are fluorescence-based microscopy systems, the sample preparation and illumination strategy are different, suggesting that they would be good techniques to compare fiber structural parameters including fiber lengths, pore size (the volume between the fibers), and branch point density (the number of fiber branches per volume). Using the same concentrations as in D.1.1, we will prepare and image fibrin gels with these two techniques. 30 μm high z-stacks will be recorded and fiber lengths, branch point density, and pore size will be quantified using Imaris and/or ImageJ, and Matlab software previously developed to measure pore size (91, 92). Similar to D.2.2, we will correlate final fiber lengths with early fibrin species and growth kinetics observed in Aim 1 to determine how these early polymerization processes culminate in the final observed diameters.

Preliminary data (not shown) collected at 3 mg/mL fibrinogen and 0.1 U/mL thrombin show a striking difference between average lengths using light sheet microscopy (25 ± 5 μm) and confocal microscopy (6.9 ± 2.4 μm), demonstrating that a careful analysis must be performed to understand the mechanisms behind these differences. Data will be collected and analyzed in at least three different gel locations for at least three biological replicates for each biochemical condition to ensure statistical rigor.

D.2.4 Alternative approaches. One limitation in using super-resolution imaging is the use of fluorescently labeled molecules. Using 100% fluorescently labeled molecules leads to aberrant fiber structures (7), so common practice is to only use ~1-5% of labeled molecules (7, 93, 94). Our preliminary data (Fig. 8), suggest that with 2% of molecules labeled, super-resolution and SEM-based fiber diameters agree well. However, to carefully test this, we could polymerize clots using identical fibrinogen concentrations, but differing percentages of labeled fibrinogen molecules to determine whether the labeling percentage effects diameter measurements. We could also compare different super-resolution microscopy techniques such as STORM and STED (Stimulated Emission Depletion) to determine whether they provide congruent answers. Finally, the best method for pore size measurements has been debated (95), so we could compare the variously proposed pore-size methods to test their similarity.

D.3 Aim 3: Determine how early clot structures affect lysis

D.3.1 Introduction and hypothesis. Previous studies suggest that fibrinolysis rates are determined by fibrin gel properties including fiber diameter and network pore size (96, 97). Because fibrin gel properties are, in turn, regulated by the polymerization processes, we hypothesize that the early stages of polymerization predetermine the eventual lytic properties of that network. However, to our knowledge, this link has not been directly established. To test this hypothesis, we will utilize both bulk and single fiber fibrinolysis assays to correlate lysis rates with polymerization processes.

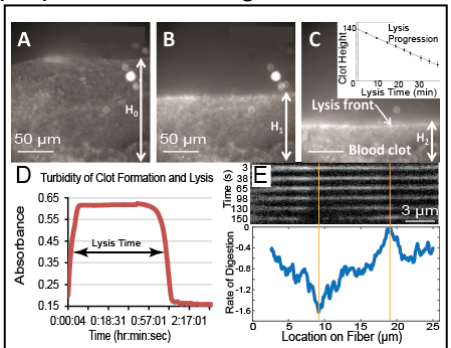

Figure 9. Clot lysis experiments. (A-C) Image series of a receding clot. The arrows H_0, H_1 and H_2 measure clot height at 0, 14 and 28 min. C-inset: Clot height vs. time; slope represents the lytic rate. (D) Turbidity measurement of clot formation and lysis, in human plasma. Clot formation results in a turbidity (absorbance) increase. Lysis starts ~70 min and results in a decrease in absorbance. E. Top: Image time-series of a single fibrin fiber lysis experiment. Images taken every 2.5 s during lysis. Bottom: Rate of digestion plot based on loss in fluorescence intensity at each location along the fiber during lysis. More negative values indicate faster digestion. Orange lines correlate two fiber locations with their local digestion rate.

D.3.2 Correlate network lysis times to stages of early fibrin assembly. To assess network lysis, we will use a turbidity-based assay and a microscopy-based assay to observe the lysis front progression. Both assays have been used in peer-reviewed publications by the applicants before (98). In a turbidity-based assay, plasminogen and tissue plasminogen activator (tPA) are added to the clotting solution and turbidity is observed over time. This assay has recently been standardized by Dr. Guthold and others, and we will follow this protocol (99). As part of our preliminary data, we have also developed a time-resolved turbidimetry assay (data not shown) that can assess fibrin fiber structures, including mass-length ratio and average fiber diameter over time during lysis. In the microscopy-based assay, a clot is formed between glass slides, plasmin is added to one side of the clot, and the clot front is then observed over time (Fig. 9). These assays will be performed for all conditions described in D.1.1. Taken together, these assays will yield clot lysis time, rate of formation, and rate of lysis in addition to the fiber properties. Rates obtained from the turbidity and microscopy-based assays will be correlated with the formation of early fibrin oligomers (D.1.2), the longitudinal and lateral fiber growth rates (D.1.4), and the rate of fiber branching (D.1.5) to determine whether these properties determine clot lysis rates.

D.3.3 Correlate single fiber lysis times to early clot parameters. To test the effects of polymerization on the lysis mechanisms of individual fibrin fibers, we will utilize a single fiber lysis assay that was developed by undergraduate students as part of the original grant (6-8). Briefly, 2% Alexa fluor™ 488-labeled fibrin fibers, which are polymerized between microprinted ridges, are subjected to lysis using either plasmin or tPA and plasminogen. Using epifluorescent widefield microscopy, time-series images of the fibers during digestion are collected, and digestion is observed as a loss in average cross-sectional fluorescence intensity. Using the troughs in the rate of digestion plots (Fig. 9E), we will quantify the locations and numbers of digestion sites in each fiber and the time it takes for a fiber to be completely cut through (the fiber cleavage rate). These assays will be performed on small networks polymerized under each of the conditions described in D.1.1. 100 fibers will be analyzed for each condition to ensure statistical robustness of results. Single fiber cleavage rates will be correlated with polymerization properties in the same way as the network rates described in D.3.2.

D.3.4 Model fibrinolysis of clots of different structures to elucidate how variations in early-stage polymerization and clot formation affect lytic outcomes. We will leverage our established multiscale model

of fibrinolysis (67) to investigate the rates and patterns of lysis of clots of different structure. Briefly, this is a stochastic model of a 3D fibrin clot (represented by a square lattice) that tracks tPA molecules as they diffuse, bind to fibers, and unbind from fibers. When a tPA molecule binds to a fiber on the macroscale, it initiates the lytic cascade on the microsale (represented by a 2D fibrin fiber cross-section) (67). We propose to adapt this model to determine the effect of structural changes due to early-stage polymerization on resulting patterns and rates of lysis. Specifically, we will tune the macroscale model parameters pore size (distance between fibers in the macroscale model) and fiber diameter to match the experimental clot structures observed from different polymerization conditions. Microscale model diameter and fraction of fibrin necessary for cleavage will also be tuned accordingly. We will record the microscale single fiber cleavage times and the macroscale lysis rate and time to 50% and 90% lysis. Additionally, we will test more (and more extreme) structures than are feasible experimentally, and ultimately propose which aspects of early-stage polymerization have the greatest impact on subsequent lysis.

D.3.5 Alternative approaches. Because the differing polymerization conditions will result in fibers of different length and diameter, we could correlate these fiber properties with the lysis rates. In microscopy assays, we could analyze the dissolution of fiber junctions, which would provide information on their internal structure, and help to differentiate between the different types of junctions and their susceptibility to lysis. In addition, using the high frame rate microscopy, we could attempt to track fibrin structures over time beginning with polymerization and ending with lysis. It is possible that for some early-stage polymerization conditions, the resulting fibrin networks will be too complicated to be accurately modeled by a square lattice with fixed-diameter fibers. In this case, we will modify the model so that different lattice edges (i.e., different fibers) have randomly assigned diameters chosen from a discrete list that is consistent with experimental data. This will require generating microscale model data for all allowable fiber diameters and accessing the appropriate distributions on the macroscale, but this will be straightforward to implement.

D.4 Opportunities for undergraduate student training

The PI and co-I's have demonstrated, strong track records of undergraduate (UG) student training. The projects in this proposal will provide training to UG students at three different universities in a wide variety of biophysical and mathematical techniques. A detailed recruitment and training plan is included in the facilities and other resources document. At ECU, one graduate student will take the lead on collecting light sheet microscopy data (Aim 1). UG students will help in developing tools to analyze the data. UG students will directly be trained on and take SEM, super-resolution STORM, and turbidimetry data in Aim 2, and UG students will take the single fiber lysis data in Aim 3. At WFU, a graduate student will take the lead on AFM, Leica THUNDER imaging, SEM imaging, and lysis experiments, and train and mentor UG students in these techniques and data analysis. At UCO, UG students will assist with model building and code writing (Aim 1) and will run model experiments and assist with data collection and analysis (Aims 1 and 3).

We will have monthly joint lab meetings where students from all three labs present data and get feedback. Students have traveled between the labs of Hudson and Guthold to receive training in the past and will continue to do so during this grant. As demonstrated in our previous grant, undergraduate students will be actively involved in paper writing and submissions. Using internal funds, we plan for a UG student from UCO to spend a week in either the Hudson or Guthold lab to understand experimental details to help mathematical modeling efforts. Students from WFU and ECU will present data at the NC Symposium on Hemostasis, an internationally known conference that is always held in North Carolina. Students from UCO will present their work at the OK-AR Section Meeting of the Mathematical Association of America and at Oklahoma Research Day. Female UG students will have the opportunity to present at the Nebraska Conference for Undergraduate Women in Mathematics.

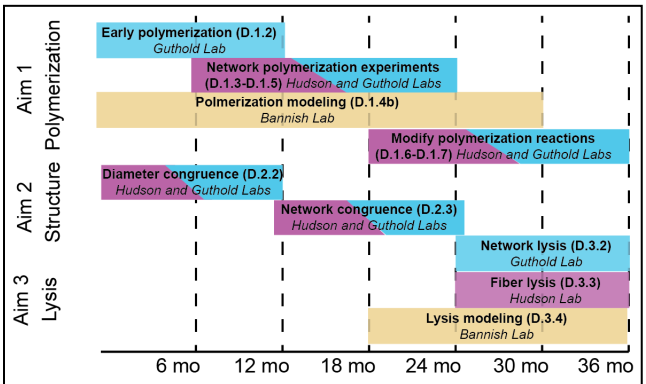

Figure 10. Timeline of proposed work.

D.5 Conclusions

The combination of multiscale experiments and modeling described in this proposal will help to bridge key knowledge gaps in our understanding of fibrin polymerization, network structure, and lysis. These experiments build off preliminary data generated from our previously successful grant and provide a fertile training ground for undergraduate and graduate students. Our interdisciplinary research team has a track record of success and is well qualified to perform the described research, in the timeline described in Fig. 10, and train the next generation of scientists. Successful completion of this proposal has the potential to aid in improved clinical diagnosis and treatment for diseases with altered fibrin polymerization and structure.

Progress Report Publication List

1. Risman, R.A., Kirby, N.C., Bannish, B.E., Hudson, N.E., Tutwiler, V. Fibrinolysis: an illustrated review. *Res Pract Thromb Haemost*. 2023 Feb 17;7(2):100081. PMID: 36942151 PMCID: PMC10024051.
2. Stoll, E.G., Cone, S.J., Lynch, S.R., Fuquay, A.T., Bannish, B.E., Hudson, N.E. Fluorescent microspheres can affect in vitro fibrinolytic outcomes. *PLoS One*. 2023 Apr 7;18(4):e0284163. PMID: 37027378 PMCID: PMC10081780.
3. Belcher, H.A., Litwa, K., Guthold, M., Hudson, N.E. The Applicability of Current Turbidimetric Approaches for Analyzing Fibrin Fibers and Other Filamentous Networks *Biomolecules.* 2022 June 9;12(6):807. PMID: 35740932 PMCID: PMC9221518.
4. Lynch, S.R., Laverty, S.M., Bannish, B.E., Hudson, N.E. Microscale structural changes of individual fibrin fibers during fibrinolysis. *Acta Biomaterialia.* 2022 Mar 15;141:114-122. PMID: 35007782 PMCID: PMC8898298.
5. Popovic, G., Kirby, N.C., Dement, T.C., Peterson, K.M., Daub, C.E., Belcher, H.A., Guthold, M., Offenbacher, A.R., Hudson N.E. Development of Transient Recombinant Expression and Affinity Chromatography Systems for Human Fibrinogen. *IJMS.* 2022 Jan 19;23(3). PMID: 35162976 PMCID: PMC8835685.
6. Bannish, B.E., Hudson N.E. The Utility and Potential of Mathematical Models in Predicting Fibrinolytic Outcomes. *Current Opinion in Biomedical Engineering.* 2021 Dec;20. PMID: 34957356 PMCID: PMC8694003.
7. Cone S.J., Fuquay A.T., Litofsky J.M., Dement T.C., Carolan C.A., Hudson N.E. Inherent fibrin fiber tension propels mechanisms of network clearance during fibrinolysis. *Acta Biomaterialia.* 2020 April 15;107:164-177. PMID: 32105833 PMCID: PMC7160043.
8. Maksudov F, Daraei A, Sesha A, Marx K, Guthold M, Barsegov V. Strength, deformability and toughness of uncrosslinked fibrin fibers from theoretical reconstruction of stress-strain curves. *Acta Biomater* 2021 Dec;136:327-342. PMID: 34606991 PMCID: PMC8627496.
9. Daraei A, Pieters M, Baker S, de Lange-Loots Z, Siniarski A, Litvinov R, Veen C, de Maat M, Weisel J, Ariens R, Guthold M. Automated Fiber Diameter and Porosity Measurements of Plasma Clots in Scanning Electron Microscopy Images. *Biomolecules* 2021 Oct 18;11(10):1536. PMID: 34680169 PMCID: PMC8533744.
10. Lee H, Bonin K, Guthold M. Human mammary epithelial cells in a mature, stratified epithelial layer flatten and stiffen compared to single and confluent cells. *Biochim Biophys ACTA-Gen* 2021 Jun;1865(6):129891. PMID: 33689830 PMCID: PMC8052296.
11. Pieters M, Guthold M, Nunes C, de Lange Z. Interpretation and Validation of Maximum Absorbance Data Obtained from Turbidimetry Analysis of Plasma Clots. *Thromb Haemost* 2020 Jan;120(1):44-54. PMID: 31752041 PMCID: PMC7369642
12. Sharpe J, Lee H, Hall A, Bonin K, Guthold M. Mechanical Properties of Electrospun, Blended Fibrinogen: PCL Nanofibers. *Nanomaterials* 2020 Sep 15;10(9):1843. PMID: 32942701 PMCID: PMC7558679.

*Note underlined authors were undergraduate students at the time that their contributions to the paper were completed

References

1. Popovic G, Kirby NC, Dement TC, Peterson KM, Daub CE, Belcher HA, Guthold M, Offenbacher AR, Hudson NE. Development of transient recombinant expression and affinity chromatography systems for human fibrinogen. *International journal of molecular sciences.* 2022 Jan 19,; 23(3): 1054. PMCID: PMC8835685.

2. Maksudov F, Daraei A, Sesha A, Marx KA, Guthold M, Barsegov V. Strength, deformability and toughness of uncrosslinked fibrin fibers from theoretical reconstruction of stress-strain curves. *Acta biomaterialia.* 2021 Dec 1,; 136: 327-342. PMCID: PMC8627496.

3. Pieters M, Guthold M, Nunes CM, de Lange Z. Interpretation and validation of maximum absorbance data obtained from turbidimetry analysis of plasma clots. *Thrombosis and haemostasis.* 2020; 120(1): 44. PMCID: PMC7369642.

4. Daraei A, Pieters M, Baker SR, de Lange-Loots Z, Siniarski A, Litvinov RI, Veen CSB, de Maat, Moniek P. M, Weisel JW, Ariëns RAS, Guthold M. Automated fiber diameter and porosity measurements of plasma clots in scanning electron microscopy images. *Biomolecules (Basel, Switzerland).* 2021 Oct 18,; 11(10): 1536. PMCID: PMC8533744.

5. Belcher HA, Litwa K, Guthold M, Hudson NE. The applicability of current turbidimetric approaches for analyzing fibrin fibers and other filamentous networks. *Biomolecules (Basel, Switzerland).* 2022 Jun 9,; 12(6): 807. PMCID: PMC9221518.

6. Cone SJ, Fuquay AT, Litofsky JM, Dement TC, Carolan CA, Hudson NE. Inherent fibrin fiber tension propels mechanisms of network clearance during fibrinolysis. *Acta Biomaterialia.* 2020 Apr 15,; 107: 164-177. PMCID: PMC7160043.

7. Lynch SR, Laverty SM, Bannish BE, Hudson NE. Microscale structural changes of individual fibrin fibers during fibrinolysis. *Acta biomaterialia.* 2022 March 15,; 141: 114-122. PMCID: PMC8898298.

8. Stoll EG, Cone SJ, Lynch SR, Fuquay AT, Bannish BE, Hudson NE. Fluorescent microspheres can affect in vitro fibrinolytic outcomes. *PloS one.* 2023 Apr 7,; 18(4): e0284163. PMCID: PMC10081780.

9. Dunn E, Ariëns R, Grant P. The influence of type 2 diabetes on fibrin structure and function. *Diabetologia.* 2005; 48(6): 1198-1206. PMCID: N/A.

10. Siniarski A, Baker SR, Duval C, Malinowski KP, Gajos G, Nessler J, Ariëns RAS. Quantitative analysis of clot density, fibrin fiber radius, and protofibril packing in acute phase myocardial infarction. *Thrombosis research.* 2021; 205: 110-119. PMCID: N/A.

11. Undas A, Slowik A, Wolkow P, Szczudlik A, Tracz W. Fibrin clot properties in acute ischemic stroke: Relation to neurological deficit. *Thrombosis research.* 2009; 125(4): 357-361. PMCID: N/A.

12. Undas A, Ariëns RAS. Fibrin clot structure and function: A role in the pathophysiology of arterial and venous thromboembolic diseases. *Arteriosclerosis, Thrombosis, and Vascular Biology.* 2011; 31(12): e88-e99. PMCID: N/A.

13. de Vries JJ, Visser C, Geers L, Slotman JA, van Kleef ND, Maas C, Bax HI, Miedema JR, van Gorp, Eric C M, Goeijenbier M, van den Akker, Johannes P C, Endeman H, Rijken DC, Kruip, Marieke J H A, de Maat, Moniek P M. Altered fibrin network structure and fibrinolysis in intensive care unit patients with COVID-19, not entirely explaining the increased risk of thrombosis. *Journal of thrombosis and haemostasis.* 2022 Jun; 20(6): 1412-1420. PMCID: PMC9115158.

14. Pretorius E, Vlok M, Venter C, Bezuidenhout JA, Laubscher GJ, Steenkamp J, Kell DB. Persistent clotting protein pathology in long COVID/post-acute sequelae of COVID-19 (PASC) is accompanied by increased levels of antiplasmin. *Cardiovascular diabetology.* 2021 Aug 23,; 20(1): 1-172. PMCID: PMC8381139.

15. Howell WH. The clotting of blood as seen with the ultramicroscope. *The American journal of physiology.* 1914 Aug 1,; 35(1): 143-149. PMCID: N/A.

16. Van Zandt Hawn C, Porter KR. The fine structure of clots formed from purified bovine fibrinogen and thrombin - a study with the electron microscope. *The Journal of Experimental Medicine.* 1947 Sep 30,; 86(4): 285-292. PMCID: PMC2135733.

17. Hall CE, Slayter HS. The fibrinogen molecule: Its size, shape, and mode of polymerization. *Journal of Biophysical and Biochemical Cytology.* 1959 Jan 25,; 5(1): 11-16. PMCID: PMC2224630.

18. Bailey K, Bettelheim FR. The clotting of fibrinogen I. the liberation of peptide material. *Biochimica et biophysica acta.* 1955; 18(4): 495-503. PMCID: N/A.

19. Bettelheim FR. The clotting of fibrinogen II. fractionation of peptide material liberated. *Biochimica et biophysica acta.* 1956; 19(1): 121-130. PMCID: N/A.

20. Janmey PA, Bale MD, Ferry JD. Polymerization of fibrin: Analysis of light-scattering data and relation to a peptide release. *Biopolymers.* 1983; 22(9): 2017-2019. PMCID: N/A.

21. Blombäck B, Hessel B, Hogg D, Therkildsen L. A two-step fibrinogen-fibrin transition in blood coagulation. *Nature (London).* 1978 Oct 12,; 275(5680): 501-505. PMCID: N/A.

22. Ferry JD. The mechanism of polymerization of fibrinogen. *Proceedings of the National Academy of Sciences - PNAS.* 1952 Jul 15,; 38(7): 566-569. PMCID: PMC1063615.

23. Fowler WE, Hantgan RR, Hermans J, Erickson HP. Structure of the fibrin protofibril. *Proceedings of the National Academy of Sciences of the United States of America.* 1981 Aug 1,; 78(8): 4872-4876. PMCID: PMC320279.

24. Krakow W, Endres GF, Siegbl BM, Schekaga HA. An electron microscopic investigation of the polymerization of bovine fibrin monomer. *Journal of molecular biology.* 1972; 71(1): 95,IN7,101-100,IN11,103. PMCID: N/A.

25. Weisel JW, Phillips Jr GN, Cohen C. The structure of fibrinogen and fibrin: II. architecture of the fibrin clot. *Annals of the New York Academy of Sciences.* 1983; 408(1): 367-379. PMCID: N/A.

26. Weisel JW, Veklich Y, Gorkun O. The sequence of cleavage of fibrinopeptides from fibrinogen is important for protofibril formation and enhancement of lateral aggregation in fibrin clots. *J Mol Biol.* 1993; 232(1): 285-297. PMCID: N/A.

27. Hantgan RR, Hermans J. Assembly of fibrin. A light scattering study. *The Journal of biological chemistry.* 1979 Nov 25,; 254(22): 11272-11281. PMCID: N/A.

28. Medved L, Ugarova T, Veklich Y, Lukinova N, Weisel J. Electron microscope investigation of the early stages of fibrin assembly: Twisted protofibrils and fibers. *Journal of molecular biology.* 1990; 216(3): 503-509. PMCID: N/A.

29. Weisel JW, Nagaswami C, Makowski L. Twisting of fibrin fibers limits their radial growth. *Proceedings of the National Academy of Sciences of the United States of America.* 1987 Dec 15,; 84(24): 8991-8995. PMCID: PMC299677.

30. Zhmurov A, Protopopova AD, Litvinov RI, Zhukov P, Weisel JW, Barsegov V. Atomic structural models of fibrin oligomers. *Structure.* 2018 Jun 5,; 26(6): 857-868.e4. PMCID: PMC6501597.

31. Zavyalova EG, Protopopova AD, Kopylov AM, Yaminsky IV. Investigation of early stages of fibrin association. *Langmuir : the ACS journal of surfaces and colloids.* 2011 Apr 19,; 27(8): 4922-4927. PMCID: N/A.

32. Hunziker EB, Straub PW, Haeberli A. A new concept of fibrin formation based upon the linear growth of interlacing and branching polymers and molecular alignment into interlocked single-stranded segments. *The Journal of Biological Chemistry.* 1990 May 5,; 265(13): 7455-7463. PMCID: N/A.

33. Hunziker EB, Straub PW, Haeberli A. Molecular morphology of fibrin monomers and early oligomers during fibrin polymerization. *Journal of ultrastructure and molecular structure research.* 1988; 98(1): 60-70. PMCID: N/A.

34. Rocco M, Molteni M, Ponassi M, Giachi G, Frediani M, Koutsioubas A, Profumo A, Trevarin D, Cardinali B, Vachette P, Ferri F, Pérez J. A comprehensive mechanism of fibrin network formation involving early branching and delayed single- to double-strand transition from coupled time-resolved X-ray/light-scattering detection. *Journal of the American Chemical Society.* 2014 Apr 9,; 136(14): 5376. PMCID: N/A.

35. Gorkun OV, Henschen-Edman AH, Ping LF, Lord ST. Analysis of A alpha 251 fibrinogen: The alpha C domain has a role in polymerization, albeit more subtle than anticipated from the analogous proteolytic fragment X. *Biochemistry.* 1998 Nov 3,; 37(44): 15434. PMCID: N/A.

36. Carr J, M E, Hermans J. Size and density of fibrin fibers from turbidity. *Macromolecules.* 1978; 11(1): 46-50. PMCID: N/A.

37. Weisel JW, Nagaswami C. Computer modeling of fibrin polymerization kinetics correlated with electron microscope and turbidity observations: Clot structure and assembly are kinetically controlled. *Biophysical Journal.* 1992; 63(1): 111-128. PMCID: PMC1262129.

38. Hantgan R, McDonagh J, Hermans J. Fibrin assembly. *Annals of the New York Academy of Sciences.* 1983; 408(1): 344-366. PMCID: N/A.

39. Hantgan R, Fowler W, Erickson H, Hermans J. Fibrin assembly: A comparison of electron microscopic and light scattering results. *Thrombosis and haemostasis.* 1980; 44(3): 119-124. PMCID: N/A.

40. Collet J, Lesty C, Montalescot G, Weisel JW. Dynamic changes of fibrin architecture during fibrin formation and intrinsic fibrinolysis of fibrin-rich clots. *Journal of Biological Chemistry.* 2003 Jun 13,; 278(24): 21331-21335. PMCID: N/A.

41. Chernysh IN, Weisel JW. Dynamic imaging of fibrin network formation correlated with other measures of polymerization. *Blood.* 2008 May 15,; 111(10): 4854-4861. PMCID: PMC2384121.

42. Chernysh IN, Nagaswami C, Weisel JW. Visualization and identification of the structures formed during early stages of fibrin polymerization. *Blood.* 2011 Apr 28,; 117(17): 4609-4614. PMCID: PMC3099577.

43. Hategan A, Gersh KC, Safer D, Weisel JW. Visualization of the dynamics of fibrin clot growth 1 molecule at a time by total internal reflection fluorescence microscopy. *Blood.* 2013 Feb 21,; 121(8): 1455-1458. PMCID: PMC3578959.

44. Blombäck B, Carlsson K, Hessel B, Liljeborg A, Procyk R, Aslund N. Native fibrin gel networks observed by 3D microscopy, permeation and turbidity. *Biochimica et biophysica acta.* 1989 Jul 27,; 997(1-2): 96. PMCID: N/A.

45. Magatti D, Molteni M, Cardinali B, Rocco M, Ferri F. Modeling of fibrin gels based on confocal microscopy and light-scattering data. *Biophysical journal.* 2017 Jan 24,; 112(2): 410. PMCID: PMC5266255.

46. Hall CE. Electron microscopy of fibrinogen and fibrin. *The Journal of biological chemistry.* 1949 Jun; 179(2): 857-865. PMCID: N/A.

47. Mosesson MW, DiOrio JP, Siebenlist KR, Wall JS, Hainfeld JF. Evidence for a second type of fibril branch point in fibrin polymer networks, the trimolecular junction. *Blood.* 1993 Sep 1,; 82(5): 1517-1521. PMCID: N/A.

48. Müller MF, Ris H, Ferry JD. Electron microscopy of fine fibrin clots and fine and coarse fibrin films: Observations of fibers in cross-section and in deformed states. *Journal of molecular biology.* 1984; 174(2): 369-384. PMCID: N/A.

49. García X, Seyve L, Tellier Z, Chevreux G, Bihoreau N, Polack B, Caton F. Aggregates dramatically alter fibrin ultrastructure. *Biophysical journal.* 2020 Jan 7,; 118(1): 172-181. PMCID: PMC6950636.

50. Carlisle CR, Sparks EA, Der Loughian C, Guthold M. Strength and failure of fibrin fiber branch points. *Journal of Thrombosis and Haemostasis.* 2010 PMCID: PMC3013622.

51. Fogelson AL, Nelson AC, Zapata-Allegro C, Keener JP. Development of fibrin branch structure before and after gelation. *SIAM journal on applied mathematics.* 2022 Jan 1,; 82(1): 267-293. PMCID: PMC9455619.

52. Fogelson AL, Keener JP. Toward an understanding of fibrin branching structure. *Physical review. E, Statistical, nonlinear, and soft matter physics.* 2010; 81(5 Pt 1): 051922. PMCID: PMC2997395.

53. Nelson AC, Kelley MA, Haynes LM, Leiderman K. Mathematical models of fibrin polymerization: Past, present, and future. *Current opinion in biomedical engineering.* 2021; 20: 100350. PMCID: N/A.

54. Wilf J, Minton AP. Soluble fibrin-fibrinogen complexes as intermediates in fibrin gel formation. *Biochemistry (Easton).* 1986 Jun 1,; 25(11): 3124-3133. PMCID: N/A.

55. Naski MC, Shafer JA. A kinetic model for the alpha-thrombin-catalyzed conversion of plasma levels of fibrinogen to fibrin in the presence of antithrombin III. *The Journal of biological chemistry.* 1991 Jul 15,; 266(20): 13003-13010. PMCID: N/A.

56. Guria GT, Herrero MA, Zlobina KE. Ultrasound detection of externally induced microthrombi cloud formation: A theoretical study. *J Eng Math.* 2010; 66(1-3): 293-310. PMCID: N/A.

57. Rukhlenko OS, Dudchenko OA, Zlobina KE, Guria GT. Mathematical modeling of intravascular blood coagulation under wall shear stress. *PLoS ONE.* 2015; 10(7): e0134028. PMCID: PMC4519339.

58. Kelley M, Leiderman K. A mathematical model of bivalent binding suggests physical trapping of thrombin within fibrin fibers. *Biophysical journal.* 2019 Oct 15,; 117(8): 1442-1455. PMCID: PMC6817721.

59. Yesudasan S, Wang X, Averett RD. Coarse-grained molecular dynamics simulations of fibrin polymerization: Effects of thrombin concentration on fibrin clot structure. *J Mol Model.* 2018; 24(5): 109-14. PMCID: N/A.

60. Yesudasan S, Wang X, Averett RD. Fibrin polymerization simulation using a reactive dissipative particle dynamics method. *Biomech Model Mechanobiol.* 2018; 17(5): 1389-1403. PMCID: PMC6139262.

61. Takeishi N, Shigematsu T, Enosaki R, Ishida S, Ii S, Wada S. Development of a mesoscopic framework spanning nanoscale protofibril dynamics to macro-scale fibrin clot formation. *J R Soc Interface.* 2021 Nov 10,; 18(184): 20210554. PMCID: PMC8580471.

62. van Kempen TS, Bogaerds AB, Peters GM, van de Vosse F. A constitutive model for a maturing fibrin network. *Biophysical Journal.* 2014 Jul 15,; 107(2): 504-513. PMCID: PMC4104056.

63. Carr Jr ME, Alving BM. Effect of fibrin structure on plasmin-mediated dissolution of plasma clots. *Blood Coagulation & Fibrinolysis.* 1995; 6(6): 567-573. PMCID: N/A.

64. Machlus KR, Cardenas JC, Church FC, Wolberg AS. Causal relationship between hyperfibrinogenemia, thrombosis, and resistance to thrombolysis in mice. *Blood.* 2011 May 5,; 117(18): 4953-4963. PMCID: PMC3100702.

65. Collet J, Park D, Lesty C, Soria J, Soria C, Montalescot G, Weisel J. Influence of fibrin network conformation and fibrin fiber diameter on fibrinolysis speed: Dynamic and structural approaches by confocal microscopy. *Arteriosclerosis, Thrombosis, and Vascular Biology: Journal of the American Heart Association.* 2000 May; 20(5): 1354-1361. PMCID: N/A.

66. Weisel JW, Veklich Y, Collet JP, Francis CW. Structural studies of fibrinolysis by electron and light microscopy. *Thrombosis and Haemostasis.* 1999; 82(2): 277-282. PMCID: N/A.

67. Bannish BE, Chernysh IN, Keener JP, Fogelson AL, Weisel JW. Molecular and physical mechanisms of fibrinolysis and thrombolysis from mathematical modeling and experiments. *Scientific reports.* 2017 Aug 7,; 7(1): 6914-11. PMCID: PMC5547096.

68. Liu W, Jawerth LM, Sparks EA, Falvo MR, Hantgan RR, Superfine R, Lord ST, Guthold M. Fibrin fibers have extraordinary extensibility and elasticity. *Science.* 2006 Aug 4,; 313(5787): 634. PMCID: PMC1950267.

69. Liu W, Carlisle CR, Sparks EA, Guthold M. The mechanical properties of single fibrin fibers. *Journal of Thrombosis and Haemostasis.* 2010 May; 8(5): 1030-1036. PMCID: PMC3010862.

70. Dutta S, Rivetti C, Gassman NR, Young CG, Jones BT, Scarpinato K, Guthold M. Analysis of single, cisplatin-induced DNA bends by atomic force microscopy and simulations. *Journal of molecular recognition.* 2018; 31(10): e2731-n/a. PMCID: PMC6168373.

71. Rivetti C, Guthold M, Bustamante C. Scanning force microscopy of DNA deposited onto mica: Equilibration versus kinetic trapping studied by statistical polymer chain analysis. *Journal of molecular biology.* 1996; 264(5): 919-932. PMCID: N/A.

72. Casini A, Brungs T, Lavenu-Bombled C, Vilar R, Neerman-Arbez M, Moerloose P. Genetics, diagnosis and clinical features of congenital hypodysfibrinogenemia: A systematic literature review and report of a novel mutation. *Journal of thrombosis and haemostasis.* 2017; 15(5): 876-888. PMCID: N/A.

73. Weisel JW, Litvinov RI. Fibrin formation, structure and properties. *Sub-cellular biochemistry.* 2017; 82: 405-456. PMCID: PMC5536120.

74. Yermolenko IS, Lishko VK, Ugarova TP, Magonov SN. High-resolution visualization of fibrinogen molecules and fibrin fibers with atomic force microscopy. *Biomacromolecules.* 2011 Feb 14,; 12(2): 370-379. PMCID: N/A.

75. Protopopova AD, Litvinov RI, Galanakis DK, Nagaswami C, Barinov NA, Mukhitov AR, Klinov DV, Weisel JW. Morphometric characterization of fibrinogen's αC regions and their role in fibrin self-assembly and molecular organization. *Nanoscale.* 2017 September 21,; 9(36): 13707-13716. PMCID: PMC6501582.

76. Protopopova AD, Barinov NA, Zavyalova EG, Kopylov AM, Sergienko VI, Klinov DV. Visualization of fibrinogen αC regions and their arrangement during fibrin network formation by high-resolution AFM. *Journal of thrombosis and haemostasis.* 2015; 13(4): 570-579. PMCID: N/A.

77. Li W, Sigley J, Pieters M, Helms C, Nagaswami C, Weisel J, Guthold M. Fibrin fiber stiffness is strongly affected by fiber diameter, but not by fibrinogen glycation. *Biophysical Journal.* 2016 Mar 29,; 110(6): 1400-1410. PMCID: PMC4816776.

78. Spiewak R, Gosselin A, Merinov D, Litvinov RI, Weisel JW, Tutwiler V, Purohit PK. Biomechanical origins of inherent tension in fibrin networks. *Journal of the mechanical behavior of biomedical materials.* 2022; 133: 105328. PMCID: PMC9434494.

79. Krzic U, Gunther S, Saunders TE, Streichan SJ, Hufnagel L. Multiview light-sheet microscope for rapid in toto imaging. *Nature Methods.* 2012 Jul 1,; 9(7): 730. PMCID: N/A.

80. Walter K, Ziesche F, inventors; Apparatus and method, particularly for microscopes and endoscopes, using baseline estimation and half-quadratic minimization for the deblurring of images. European Patent Office patent WO/2019/185174. 2019 March 3.

81. Houser JR, Hudson NE, Ping L, O'Brien ET, Superfine R, Lord ST, Falvo MR. Evidence that αC region is origin of low modulus, high extensibility, and strain stiffening in fibrin fibers. *Biophysical Journal.* 2010; 99(9): 3038-3047. PMCID: PMC2965937.

82. Guy RD, Fogelson AL, Keener JP. Fibrin gel formation in a shear flow. *Mathematical medicine and biology.* 2007; 24(1): 111-130. PMCID: N/A.

83. Nellenbach K, Kyu A, Guzzetta N, Brown AC. Differential sialic acid content in adult and neonatal fibrinogen mediates differences in clot polymerization dynamics. *Blood advances.* 2021 Dec 14,; 5(23): 5202-5214. PMCID: PMC9153052.

84. Bowley SR, Lord ST. Fibrinogen variant BbetaD432A has normal polymerization but does not bind knob "B". *Blood.* 2009 Apr 30,; 113(18): 4425. PMCID: PMC2676095.

85. Schneider CA, Rasband WS, Eliceiri KW. NIH image to ImageJ: 25 years of image analysis. *Nature methods.* 2012; 9(7): 671-675. PMCID: PMC5554542.

86. Shah GA, Nair CH, Dhall DP. Comparison of fibrin networks in plasma and fibrinogen solution. *Thrombosis research.* 1987 Feb 1,; 45(3): 257-264. PMCID: N/A.

87. Carr ME. Fibrin formed in plasma is composed of fibers more massive than those formed from purified fibrinogen. *Thrombosis and haemostasis.* 1988 Jun 16,; 59(3): 535-539. PMCID: N/A.

88. Gillespie DT. Exact stochastic simulation of coupled chemical reactions. *Journal of physical chemistry (1952).* 1977 Dec 1,; 81(25): 2340-2361. PMCID: N/A.

89. Pinelo JEE, Manandhar P, Popovic G, Ray K, Tasdelen MF, Nguyen Q, Iavarone AT, Offenbacher AR, Hudson NE, Sen M. Systematic mapping of the conformational landscape and dynamism of soluble fibrinogen. *Journal of thrombosis and haemostasis.* 2023; 21(6): 1529-1543. PMCID: N/A.

90. Ryan EA, Mockros LF, Weisel JW, Lorand L. Structural origins of fibrin clot rheology. *Biophysical Journal.* 1999; 77(5): 2813-2826. PMCID: PMC1300553.

91. Molteni M, Magatti D, Cardinali B, Rocco M, Ferri F. Fast two-dimensional bubble analysis of biopolymer filamentous networks pore size from confocal microscopy thin data stacks. *Biophysical Journal.* 2013 Mar 5,; 104(5): 1160-1169. PMCID: PMC3870948.

92. Münster S, Fabry B. A simplified implementation of the bubble analysis of biopolymer network pores. *Biophysical Journal.* 2013 Jun 18,; 104(12): 2774-2775. PMCID: PMC3686353.

93. Li W, Sigley J, Baker SR, Helms CC, Kinney MT, Pieters M, Brubaker PH, Cubcciotti R, Guthold M. Nonuniform internal structure of fibrin fibers: Protein density and bond density strongly decrease with increasing diameter. *BioMed Research International.* 2017 Jan 1,; 2017: 6385628-13. PMCID: PMC5654258.

94. Tutwiler V, Singh J, Litvinov RI, Bassani JL, Purohit PK, Weisel JW. Rupture of blood clots: Mechanics and pathophysiology. *Science advances.* 2020 Aug 1,; 6(35): eabc0496. PMCID: PMC7449685.

95. Molteni M, Magatti D, Cardinali B, Rocco M, Ferri F. Response to “A simplified implementation of the bubble analysis of Biopolymer networks pores”. *Biophysical Journal.* 2013 Jun 18,; 104(12): 2776-2777. PMCID: PMC3686351.

96. Bannish BE, Hudson NE. The utility and potential of mathematical models in predicting fibrinolytic outcomes. *Current opinion in biomedical engineering.* 2021; 20: 100337. PMCID: PMC8694003.

97. Hudson NE. Biophysical mechanisms mediating fibrin fiber lysis. *BioMed Research International.* 2017 Jan 1,; 2017 PMCID: PMC5467299.

98. Li W, Li R, Lucioni T, Bonin K, Cho SS, Guthold M. Stretching single fibrin fibers hampers their lysis. *Acta Biomaterialia.* 2017 Sep 15,; 60: 264-274. PMCID: N/A.

99. Pieters M, Philippou H, Undas A, de Lange Z, Rijken D, Mutch NJ. An international study on the feasibility of a standardized combined plasma clot turbidity and lysis assay: Communication from the SSC of the ISTH. *Journal of thrombosis and haemostasis.* 2018; 16(5): 1007-1012. PMCID: N/A.